Journal of Nuclear Materials 396 (2010) 32–42

Contents lists available at ScienceDirect

Journal of Nuclear Materials

journal homepage: www.elsevier.com/locate/jnucmat

# Relationship between changes in the crystal lattice strain and thermal conductivity of high burnup $UO_2$ pellets

Masaki Amaya [a,*], Jinichi Nakamura [a], Toyoshi Fuketa [a], Yuji Kosaka [b]

[a] Fuel Safety Research Group, Nuclear Safety Research Center, Japan Atomic Energy Agency, Tokai-mura, Naka-gun, Ibaraki 319-1195, Japan
[b] Nuclear Development Corporation, 622-12, Funaishikawa, Tokai-mura, Naka-gun, Ibaraki 319-1111, Japan

ARTICLE INFO

*Article history:*
Received 13 July 2009
Accepted 9 October 2009

ABSTRACT

Two kinds of disk-shaped $UO_2$ samples (4 mm in diameter and 1 mm in thickness) were irradiated in a test reactor up to about 60 and 130 GWd/t, respectively. The microstructures of the samples were investigated by means of optical microscopy, scanning electron microscopy/ electron probe micro-analysis (SEM/EPMA) and micro-X-ray diffractometry. The measured lattice parameters tended to be considerably smaller than the reported values, and the typical cauliflower structure which is often observed in high burnup fuel pellet is hardly seen in these samples. Thermal diffusivities of the samples were also measured by using a laser flash method, and their thermal conductivities were evaluated by multiplying the heat capacity of unirradiated $UO_2$ and sample densities. While the thermal conductivities of sample 2 showed recovery after being annealed at 1500 K, those of sample 4 were not clearly observed even after being annealed at 1500 K. These trends suggest that the amount of accumulated irradiation-induced defects depends on the irradiation condition of each sample. From the comparison of the changes in the lattice parameter and strain energy density before and after the thermal diffusivity measurements, it is likely that the thermal conductivity recovery in the temperature region from 1200 to 1500 K is related to the migration of dislocation.



## 1. Introduction

The microstructural changes which are called "rim structure" are often observed at the periphery of high burnup light water reactor (LWR) fuel pellets. In the rim structure, coarsened bubbles form, and due to this, local porosity increases. On the surface of the coarsened bubble, the cauliflower structure which consists of small sub-divided grains is observed. Since it is considered that the coarsened bubble contains high pressure fission gas, the rim structure region becomes a possible source of fission gas release in high burnup fuel pellets during normal operation or transient conditions. In order to promote the burnup extension of LWR fuel, it is important and necessary to clarify the characteristics and formation mechanisms of the rim structure.

The accumulation of irradiation-induced defects and fission gas during irradiation is one of the probable causes of rim structure formation. The temperature and burnup conditions in which the rim structure forms have been investigated by several groups, and it was reported that the thresholds were located at about 1400 K and 70 GWd/t, respectively [1]. Recently, the authors [2,3] reported lattice parameters, non-uniform strains and crystallite size in $UO_2$ fuel pellets irradiated in the burnup region from 40 to about 70 GWd/t by means of X-ray diffractometry. Although they discussed the strain energy density changes which were evaluated from the uniform and non-uniform strains in the crystallite in connection with the accumulation of dislocations and found a relationship between them, the formation mechanism of the rim structure has not been fully explained yet.

In this study, burnup and irradiation temperature effects on the changes in crystallite size and non-uniform strain are investigated based on the X-ray diffractometry results of the disk-shaped $UO_2$ samples which were irradiated up to high burnup under various irradiation conditions in a test reactor. Thermal conductivities of the samples are also measured in order to investigate temperature effects on the recovery of irradiation-induced defects. Based on the results of X-ray diffraction and thermal conductivity measurements, the relationship between changes in the crystal lattice strain and thermal conductivity of high burnup $UO_2$ pellets are discussed.

## 2. Experimental

### 2.1. Preparation of irradiation samples

Disk-shaped pellet samples (~4 mm in diameter and ~1 mm in thickness) were prepared by a sintering method. The fabrication

* Corresponding author. Tel.: +81 29 282 6386; fax: +81 29 282 5429.
*E-mail address:* amaya.masaki@jaea.go.jp (M. Amaya).

0022-3115/$ - see front matter © 2009 Elsevier B.V. All rights reserved.
doi:10.1016/j.jnucmat.2009.10.049

process was as follows: $UO_2$ powder was pressed into green pellets (~5 mm in diameter and ~1.3 mm in thickness). The green pellets were sintered at about 2100 K for 8 h under a reducing atmosphere of Ar–5%$H_2$.

The details of the sample fabrication conditions and sample characteristics are summarized in Table 1. The densities of the obtained pellets were 94–95 %TD (TD: theoretical density of $UO_2$.).

### 2.2. Irradiation test

A disk-shaped pellet was put into a sample holder of molybdenum in order to reduce temperature distribution along the radial and axial directions of the pellet. Thereafter, a fuel pin was prepared by sealing six sample holders into a fuel cladding of Nb–1%Zr with a fill gas of 1 bar of He. Five fuel pins were aligned in the center of irradiation capsule BRF-31H. The overviews of the sample holder and irradiation capsule are shown in Fig. 1. A thermocouple was located on the cladding surface at the middle of each sample holder stack, and the cladding surface temperature was measured continuously during irradiation.

Power histories of the two fuel pins are summarized in Fig. 2. Samples 1 and 2 and samples 3 and 4 were sealed into fuel pins 1 and 2, respectively, and the fuel pins 1 and 2 were irradiated at power levels of 100–200 and 200–400 W/cm, respectively, in the test reactor JRR-3 at Japan Atomic Energy Agency (JAEA). The respective average burnups were evaluated as 126 and 60 GWd/t by using the nuclear calculation code SRAC-95 [4].

Target irradiation temperatures of fuel pins 1 and 2 were 873 and 1273 K, respectively. However, it is probable that the actual irradiation temperatures were higher than these target temperatures: the measured cladding surface temperatures of fuel pins 1 and 2 had been kept at about 923 and 1113 K, respectively, during the irradiation.

After the irradiation test, a puncture test was performed on each fuel pin.

### 2.3. Optical and scanning electron microscopy (SEM) and electron probe micro-analysis (EPMA)

The sample microstructures were examined by optical and scanning electron microscopy. The microstructures on the as-polished and etched surfaces were observed.

In order to investigate the radial burnup profiles in the samples, the fission product of Nd which was retained in the fuel pellets was analyzed by electron probe micro-analysis (EPMA) with an electron beam diameter of 1 μm. The element Nd is often used as a burnup index because Nd is one of the elements that is soluble in the $UO_2$ matrix and hardly moves during irradiation.

The radial profiles of Xe were also investigated in order to know how the retained fission gas be distributed in the samples.

### 2.4. Thermal conductivity measurements

Thermal conductivities of irradiated $UO_2$ samples were measured by a laser flash method. The apparatus has been described elsewhere in detail [5]. A sample is held on the knife-edge in the sample cell of tantalum. The sample is heated using a tungsten mesh heater in a vacuum of less than $2 \times 10^{-3}$ Pa. After the sample has been kept at a desired temperature for an appropriate time, a ruby laser beam is irradiated on one side of the sample in order to induce thermal energy into the sample. The temperature response at the other side of the sample is measured using an InSb infrared sensor. The measurements are carried out three times at each temperature step.

The sample weights and thicknesses were measured before the thermal diffusivity measurements. The sample thicknesses of sample 4 were also measured after the thermal diffusivity measurements. The measured thicknesses are summarized in Table 1.

The thermal diffusivity of each sample was calculated from its rear-surface temperature response by the "logarithmic method" [6]. The "curve fitting method" [7] was also used to analyze the temperature responses in order to check the thermal diffusivity obtained by the logarithmic method and confirm that the values which were evaluated by using both methods agreed well.

Thermal conductivities of the samples were estimated using the following formula:

$$\lambda_M = \alpha_M C_p \rho_M, \quad (1)$$

where $\lambda_M$ is the thermal conductivity of the sample; $\alpha_M$, the thermal diffusivity of the sample obtained from thermal diffusivity measurements; $C_p$, the specific heat capacity; and $\rho_M$ the density of the sample. The specific heat capacity of the irradiated $UO_2$ samples was assumed to be the same as that of unirradiated $UO_2$ [8] because impurity effects on the specific heat capacity is small.

**Table 1**
Sample fabrication conditions and sample characteristics for thermal diffusivity measurement.

| Sample No. | $^{235}$U enrichment (%) | Sintering temperature (K) | Sintering time (h) | Sintering atmosphere |
|---|---|---|---|---|
| *(a) Fabrication conditions* | | | | |
| 1 and 2 | 9.010 | 2173 | 8 | Ar–5%$H_2$ |
| 3 and 4 | 19.751 | 2073 | | |

| | Fuel pin No. | Target irradiation temperature (K) |
|---|---|---|
| *(b) Irradiation conditions* | | |
| 1 and 2 | 1 | 873 |
| 3 and 4 | 2 | 1273 |

| | At fabrication | | | | After irradiation | | | |
|---|---|---|---|---|---|---|---|---|
| | Diameter (mm) | Thickness (mm) | Density (%TD) | Grain size (μm) | Burnup[a] (GWd/t) | Thickness[b] (mm) | Density[c] (g/cm$^3$) | Porosity[d] (%) |
| *(c) Sample characteristics for thermal diffusivity measurement* | | | | | | | | |
| 2 | 4.0 | 1.2 | 94.4 | 8 | 60 | 1.185 (–) | 10.09 | 5.96 |
| 4 | 3.9 | 1.2 | 95.3 | 8 | 126 | 1.256 (1.260) | 9.69 | 8.06 |

[a] The values were estimated from nuclear calculation.
[b] The values in the parentheses are the thickness measured after thermal diffusivity measurements. As for sample 2, the thickness could not be measured after thermal diffusivity measurement because the sample cracked when the sample was annealed at 1600 K.
[c] Values of sibling disk samples (samples 1 and 3) which were irradiated in the same fuel pins.
[d] Theoretical densities of samples 2 and 4 were estimated as 10.73 and 10.54 g/cm$^3$ in consideration of the mass decrease due to the nuclear fission of $^{235}$U and the burnup dependence of lattice parameter change in the soluble FPs-doped $UO_2$ [15].

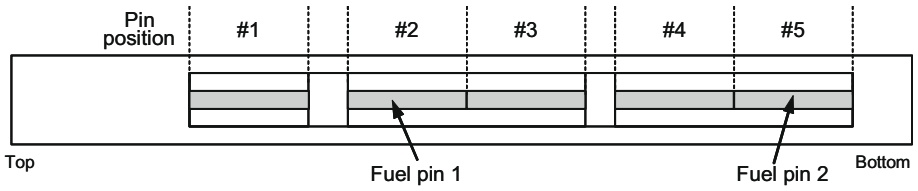


(a) Pin position in the irradiation capsule BRF-31H

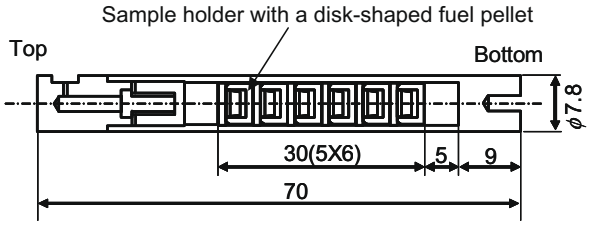


(b) Fuel pin structure

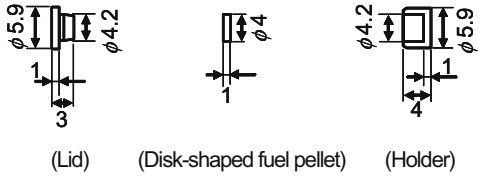


(c) Sample holder and disk-shaped fuel pellet

**Fig. 1.** Overview of the sample holder and irradiation capsule.

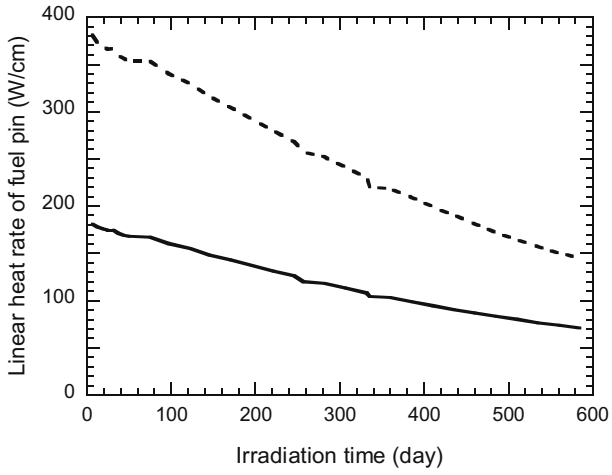


**Fig. 2.** Power histories of fuel pins —— : pin 1, – – –: pin 2.

Thermal diffusivity measurements were performed in the following sequence in consideration of the reported results of X-ray diffraction, TEM observations and thermal conductivity measurements [9,10].

Run 1: from room temperature to 700 K.
Run 2: from room temperature to 1200 K.
Run 3: from room temperature to 1500 K.
Run 4: from room temperature to 1800 K.

Since it was found that samples 2 and 4 cracked at 1600 and 1800 K, respectively, the thermal diffusivity could not be measured beyond these temperatures.

### 2.5. Measurement of lattice parameter and crystallite size

#### 2.5.1. X-ray diffractometry

X-ray diffraction measurements on irradiated $UO_2$ pellets were carried out by using a micro-X-ray diffractometer (RAD-3X type, Rigaku Corp.) with Ni-filtered Cu-Kα radiation. The measurement part of the apparatus is set in a hot cell and can be controlled from outside of the cell. The sample was placed on the *X–Y* stage of the measurement part and the position of the X-ray radiation was monitored by a TV camera. The accelerating voltage and current were 40 kV and 40 mA, respectively. The diameter of the X-ray radiation area on the sample was about 0.5 mm. The diffraction angle of the goniometer was calibrated from the measurement results of a Si standard powder sample. The accuracy of the diffraction angle was better than ±0.006° in $2\theta$ above 75°. Fig. 3 shows the X-ray diffractometry position (shown as the white box) on the axial cross-sectional surface of each sample.

#### 2.5.2. Measurement of lattice parameter, non-uniform strain and crystallite size

The lattice parameter and diffraction peak broadening (the increase of the full width at half maximum (FWHM) of diffraction peak) of the irradiated $UO_2$ pellets were evaluated from the results of X-ray diffractometry. The lattice parameter was obtained by least-squares calculations using seven diffraction lines between 75 and 130° in $2\theta$ based on Cohen's method. The scanning speed of the goniometer was 0.25° $min^{-1}$. The error in the obtained lattice parameter was less than ±0.1 pm.

Since the obtained diffraction peak was the sum of peaks due to Cu-K$\alpha_1$ and Cu-K$\alpha_2$ lines, it was necessary to separate these two peaks prior to peak broadening evaluation. The mixed peak resulting from Cu-K$\alpha_1$ and Cu-K$\alpha_2$ lines was separated by using the quasi-Voigt function and the difference of wave length between

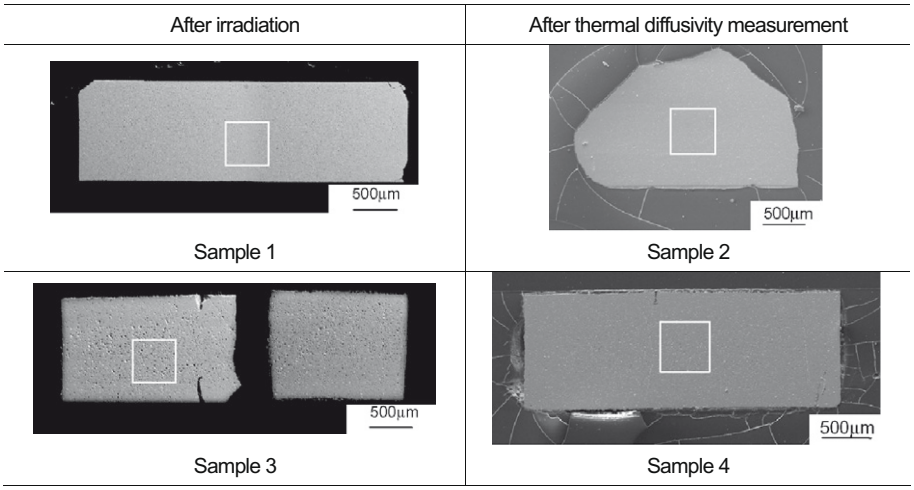


**Fig. 3.** X-ray diffractometry position on axial the cross-sectional surface of each sample.

Cu-K$\alpha_1$ and Cu-K$\alpha_2$ lines [11]. In addition, measured peak broadening contained the broadening due to the optical system arrangement of the apparatus. The latter effect on measured peak broadening was corrected based on the measurement results of the unirradiated $UO_2$ sample.

Non-uniform strain and crystallite size in a sample were evaluated by using the Williamson–Hall method [12]. According to this method, the non-uniform strain and crystallite size in the sample can be expressed as follows:

$$\beta\cos\theta = \frac{k\lambda}{D_x} + 2\eta\sin\theta \tag{2}$$

where $\beta$ is the peak broadening corrected for the systematic broadening in $2\theta$; $\theta$, the diffraction angle; $\lambda$, the X-ray wave length; $D_x$, the crystallite size; and $\eta$, the non-uniform strain. The coefficient $k$ is 0.9 when the FWHM of the peak is used as the index of broadening, and the diffraction peak and wave length of Cu-K$\alpha_1$ were used for calculation. The non-uniform strain and crystallite size were obtained by least-squares calculations using twelve diffraction peaks between 45 and 130° in $2\theta$.

## 3. Results

### 3.1. Fuel pin puncture test results

Table 2 summarizes the puncture test results of the fuel pins. In the table, fission gas releases (FGRs) were evaluated based on the total volume and composition of inner gas, fuel weight in the fuel pin and the generated gas volumes of $^{83}$Kr, $^{131}$Xe, $^{132}$Xe and $^{136}$Xe during the irradiation test. The generated gas volumes were evaluated using the codes SRAC-95 [4] and ORIGEN-2 [13].

Regarding fuel pin 1, neither krypton nor xenon was detected in the inner gas. Accordingly, it is considered that the fission gas release from the disk fuel pellets in fuel pin 1 was negligible. On the other hand, the fission gas release in fuel pin 2 was estimated as about 70%. This result indicates that the irradiation temperature of fuel pin 2 was considerably higher than the target temperature, and most fission gas was released during the irradiation test.

### 3.2. Ceramography and SEM observation results of disk fuel samples

Fig. 4 shows the SEM observation results of the samples. Regarding sample 1, since small pores which formed at fabrication can be observed, it is considered that the sample did not experience so high temperature as to causes FP gas bubble growth.

As seen in the micrographs of sample 3, many large intra- and inter-granular bubbles are precipitated in the whole of the sample. As mentioned above, the measured cladding temperature of fuel pin 2 was about 1113 K. Based on the dimensions of fuel pin, the physical properties of the unirradiated materials of the fuel pin, the linear heat rates during the irradiation and the composition of pin-inner gas which was obtained from puncture test, the surface and center temperatures of the disk fuel pellet of fuel pin 2 were estimated as about 1573 and 1673 K, respectively.[1] It is well-known that the precipitation of large intra- and inter-granular bubbles occurs in this temperature range, and the characteristics of the micrographs observed in sample 3 agree well with the features which the temperature estimation results suggest. It is also considered that the high fission gas release of fuel pin 2 was due to the high irradiation temperature above 1600 K.

In both samples, the pore inner surface is quite smooth, and the typical cauliflower structure is not clearly observed. Accordingly, it is likely that the rim structure did not form in these samples.

### 3.3. Radial profiles of burnup and retained fission gas in the samples

Fig. 5 shows the characteristic X-ray intensity profiles of Nd and Xe along the radial directions of samples 1 and 3. As seen in the figures, it is considered that the burnup profile along the radial direction of each sample is flat because the Nd concentration profile corresponds to a burnup profile in the sample. The radial profiles of Xe are also flat in both samples.

### 3.4. Thermal diffusivities and thermal conductivities of samples

Measured thermal conductivities of samples were normalized to the values of 96.5%TD (TD: theoretical density) by using the following Loeb's formula:

$$\lambda_n = \lambda_m(1 - 0.035\varepsilon)/(1 - \varepsilon P) \tag{3}$$

where $\lambda_n$ is the thermal conductivity normalized to the value of 96.5%TD; $\lambda_m$, the measured thermal conductivity; $\varepsilon$, the parameter which expresses the effect of pore shape on the thermal conductivity of pellet; and $P$, the porosity evaluated from the measured sample density. The parameter $\varepsilon$ is expressed as follows [14]:

[1] In consideration of pellet thermal conductivity degradation due to irradiation [10], it is probable that the actual temperatures of the disk fuel pellet were higher than these estimated temperatures.

**Table 2**
Puncture test results of the fuel pins.

| Fuel pin No. | Average burnup* (GWd/t) | Fuel weight at fabrication (g) | Total volume of pin-inner gas at STP ($cm^3$) | Volume ratios in the pin-inner gas (%) Kr | Xe | Released gas volume ($cm^3$) |
|---|---|---|---|---|---|---|
| *(a) Puncture results* | | | | | | |
| 1 | 60 | 0.9133 | 0.3 | N.D. | N.D. | N.D. |
| 2 | 126 | 0.9064 | 2.7 | 9.24 | 67.85 | 2.1 |

| | Released gas volume at STP ($x10^{-2}$ $cm^3$) (Fission gas release (%)) | | | | Generated gas volume at STP ($x10^{-2}$ $cm^3$) | | | | Averaged fission gas release (%) |
|---|---|---|---|---|---|---|---|---|---|
| | $^{83}Kr$ | $^{131}Xe$ | $^{132}Xe$ | $^{136}Xe$ | $^{83}Kr$ | $^{131}Xe$ | $^{132}Xe$ | $^{136}Xe$ | |
| *(b) Gas composition analysis results* | | | | | | | | | |
| 1 | N.D. (~0) | N.D. (~0) | N.D. (~0) | N.D. (~0) | 1.97 | 11.7 | 22.8 | 56.5 | ~0 |
| 2 | 3.07 (73.4) | 16.1 (66.9) | 35.9 (75.4) | 77.5 (65.7) | 4.18 | 24.1 | 47.6 | 117.9 | 70 |

N.D.: Not detected.
* Values based on nuclear calculation results.

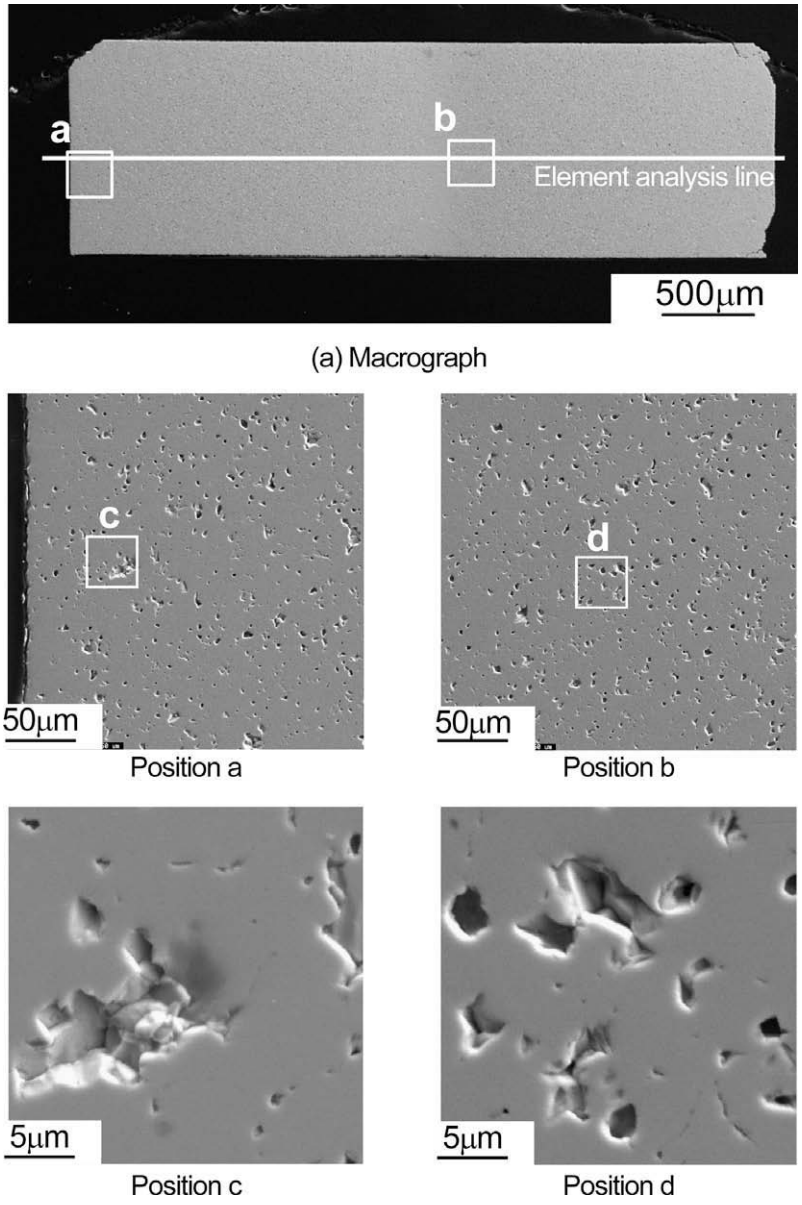


**Fig. 4a.** SEM observation results of sample 1.

$$\varepsilon = 2.6 - 5 \times 10^{-4}(T - 273.15) \quad (4)$$

where $T$ is the temperature in K.

Measured thermal diffusivities and normalized thermal conductivities of samples 2 and 4 are shown in Figs. 6 and 7, respectively. In the figures, the thermal diffusivities and thermal

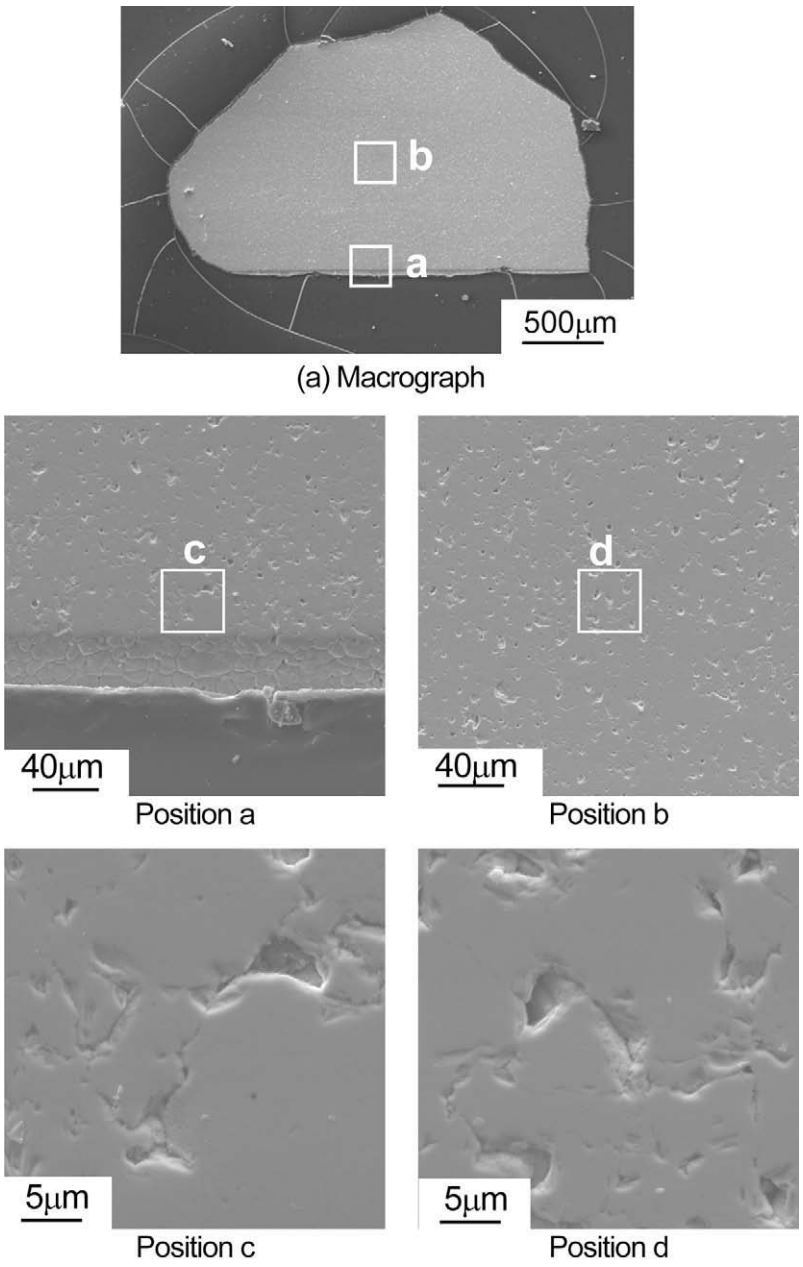


**Fig. 4b.** SEM observation results of sample 2.

conductivities of unirradiated $UO_2$ [15] are shown for comparison. In the figures of thermal conductivities, the values calculated by using the formula for irradiated $UO_2$ pellets [10,16] are also shown.

As seen in the figures, the measured values of samples 2 and 4 are lower than the values of unirradiated $UO_2$. While the thermal diffusivity of sample 2 showed recovery after the sample experienced a temperature of about 1500 K, sample 4 did not show recovery even after the sample was annealed at about 1500 K.

### 3.5. Lattice parameter change

The burnup dependence of the lattice parameter of irradiated $UO_2$ samples is shown in Fig. 8. The lattice parameters of irradiated $UO_2$ reported by several groups [2,17–23] are also presented for comparison. As seen in the figure, the measured lattice parameters of this study tend to be lower than the reported values. It is considered that these tendencies are mainly due to the effect of irradiation temperature: this implies that a part of the irradiation-induced defects recovered during the irradiation experiment.

### 3.6. Changes in non-uniform strain and crystallite size

The burnup dependences of non-uniform strain and crystallite size in irradiated $UO_2$ samples are shown in Fig. 9. In the figure, other reported values [2] are also shown for comparison.

The crystallite sizes of samples 1 and 3 are about 100 nm. These sizes are close to the reported size of the sub-divided and/or recrystallized grains in the rim structure [24]. From the comparison between the values of sample 1 and those of sample 2, it is found that the non-uniform strain and crystallite size increase after annealing at 1600 K. On the other hand, while the non-uniform strain of sample 4 decreases compared to that of sample 3, the crystallite size hardly changes. The crystallite sizes of samples 3 and 4 are about 100 nm irrespective of sample annealing.

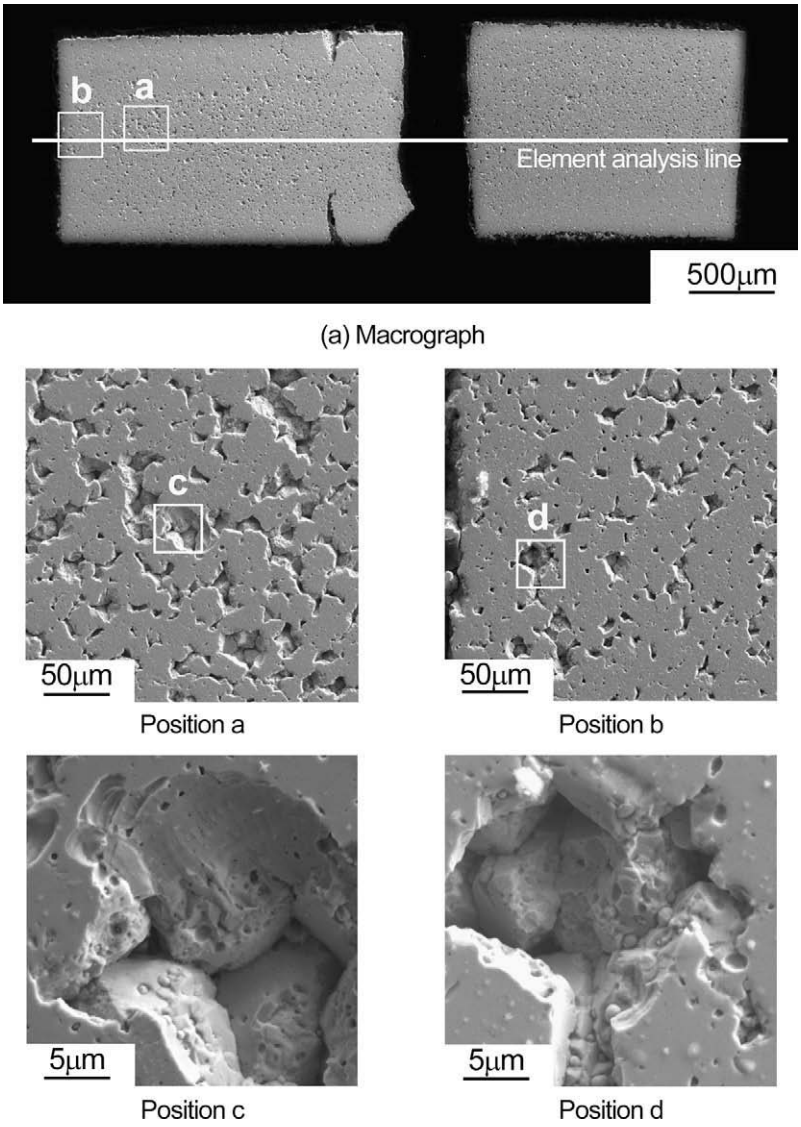


**Fig. 4c.** SEM observation results of sample 3.

### 3.7. Strain energy density in irradiated $UO_2$ sample

The strain energy density which is accumulated in irradiated $UO_2$ samples can be expressed as the sum of the strain energy densities due to crystal lattice strain and the non-uniform strain occurring between crystallites. The total strain in an irradiated sample can be divided into crystal lattice strain ($\varepsilon_c$) and non-uniform strain ($\varepsilon_{nu}$):

$$\varepsilon_{tot} = \varepsilon_c + \sqrt{\frac{2}{\pi}}\varepsilon_{nu} \tag{5}$$

The crystal lattice strain $\varepsilon_c$ is evaluated from the lattice parameter changes between irradiated and simulated soluble FPs-doped $UO_2$ as follows:

$$\varepsilon_c = \left(\frac{a - a_{FP}}{a_{FP}}\right) \tag{6}$$

where $a$ is the lattice parameter of the irradiated sample; and $a_{FP}$, the lattice parameter of soluble FPs-doped $UO_2$ with a simulated burnup of the irradiated sample [21].

It is considered that the strain occurring in an irradiated $UO_2$ sample is isotropic because the lattice structure of the $UO_2$ is fluorite and a preferred orientation was not clearly observed in non-uniform strain. Accordingly, the strain energy density, $U$, can be evaluated as follows:

$$U = \frac{3}{2}E\varepsilon_{tot}^2 \tag{7}$$

where $E$ is the Young modulus.

Fig. 10 shows the burnup dependence of strain energy density for irradiated $UO_2$ samples. In the figure, other reported values [2] are also shown for comparison. As seen in the figure, the obtained strain energy densities of all samples tend to be lower than the reported values even before the samples were annealed at high temperature.

## 4. Discussion

### 4.1. Thermal conductivity changes in irradiated $UO_2$ samples

As seen in Fig. 7, while sample 2 showed thermal conductivity recovery after being annealed at 1500 K, sample 4 did not show clear thermal conductivity recovery even after annealing at about 1500 K. In addition, the thermal conductivity recovery at about 1100 K

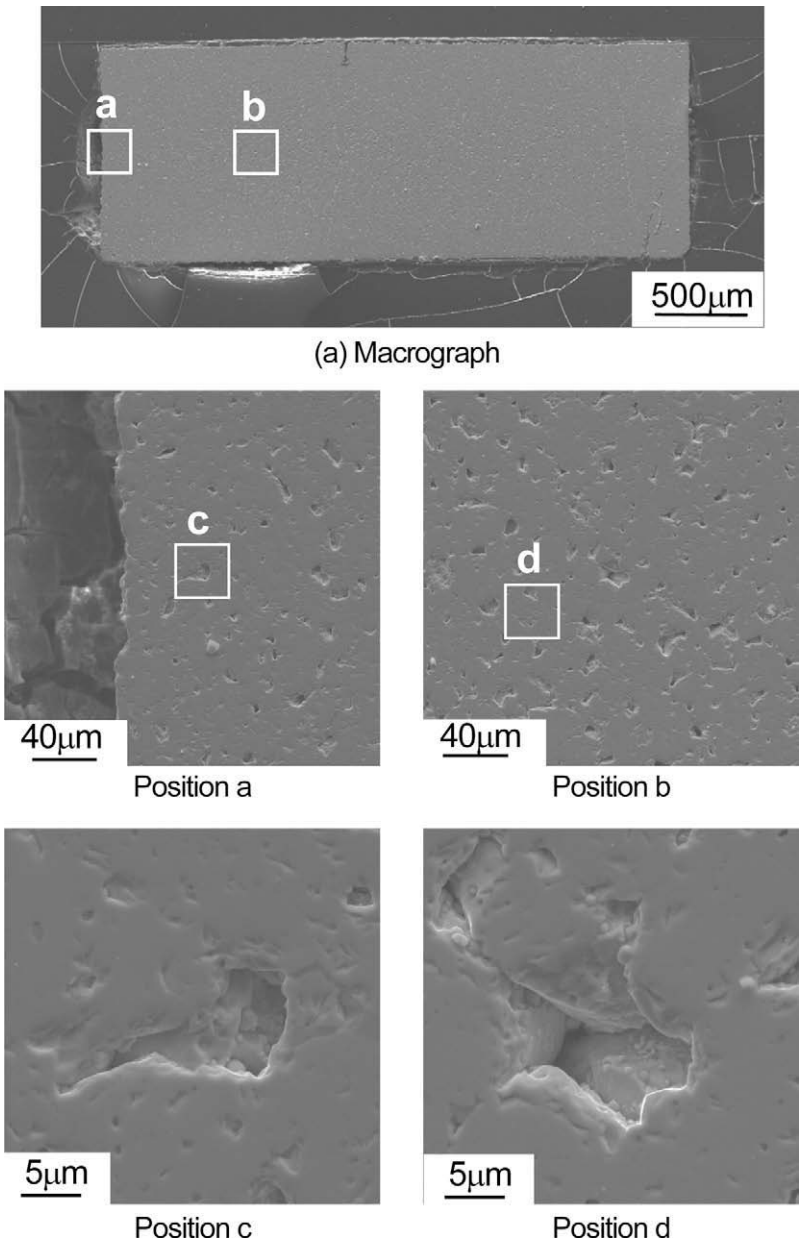


**Fig. 4d.** SEM observation results of sample 4.

which has been reported in the references [5,10] could not be seen in either sample. Since it is considered that the recovery stage at about 1100 K corresponds to point defect recovery [9], it is likely that the two samples in this study hardly contain point defects.

Nogita et al. [9] reported that broadenings of the X-ray diffraction peak from the (620) plane of $UO_2$ slightly increased after irradiated $UO_2$ pellets were annealed at 1123 K and rapidly decreased in the annealing temperature range above 1400 K. Since the broadening of the X-ray diffraction peak is caused by the non-uniform strain of crystallite and crystallite size, it is probable that the thermal conductivity recovery of sample 2 after being annealed at 1500 K is related to the changes in non-uniform strain of the crystallite and crystallite size due to sample annealing.

### 4.2. Strain energy density changes in irradiated $UO_2$ samples

According to the results of TEM (transmission electron microscopy) observations by Nogita et al. [25], dislocation densities in irradiated $UO_2$ increased in the range up to 44 GWd/t and saturated due to dislocation tangles, and it may be appropriate to consider that the formed dislocation is mainly an edge dislocation from its appearance and behavior [2,25].

Elastic strain energy density of edge dislocation per unit length, $U_{dis}$, is expressed as follows:

$$U_{dis} = U_{dis1} + U_{dis2} \tag{8}$$

where $U_{dis1}$ and $U_{dis2}$ are the elastic strain energy densities in the outside and inside of the edge dislocation core, respectively. The terms of $U_{dis1}$ and $U_{dis2}$ can be expressed as [26]:

$$U_{dis1} = \frac{\mu b^2}{4\pi(1-\nu)} \ln\frac{r_1}{r_0} \tag{9}$$

$$U_{dis2} = \frac{\mu b^2}{8\pi(1-\nu)^2} \tag{10}$$

where $\mu$ is the shear modulus; $b$, the Burgers vector; $\nu$, the Poisson ratio; $r_1$, the radius of stress region affected by dislocations; and $r_0$, the radius of the edge dislocation core.

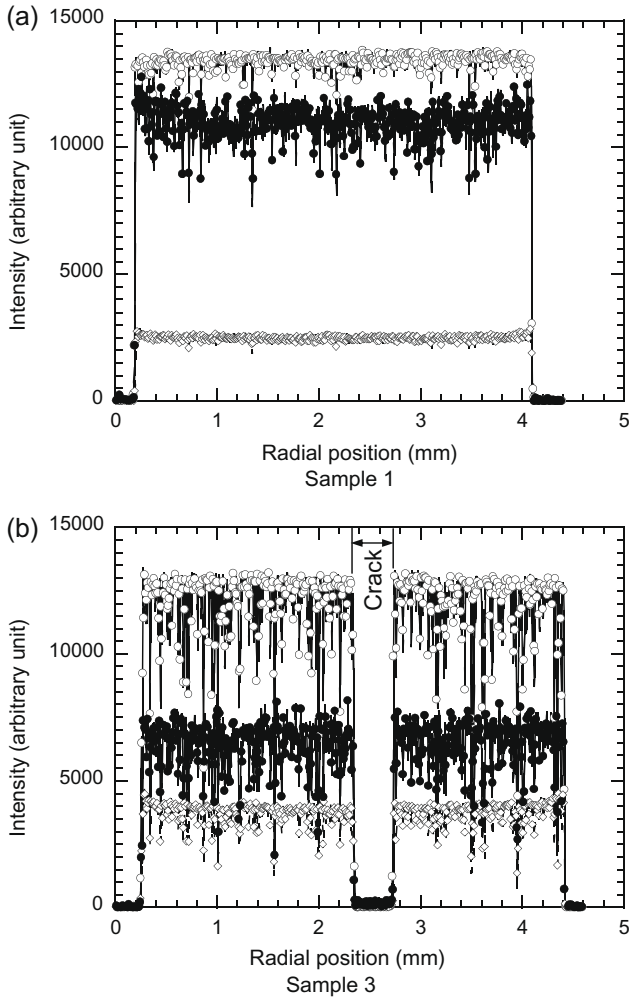


**Fig. 5.** Radial profiles of the relative concentrations of U, Nd and Xe in the samples. ○: U, ◇: Nd, ●: Xe.

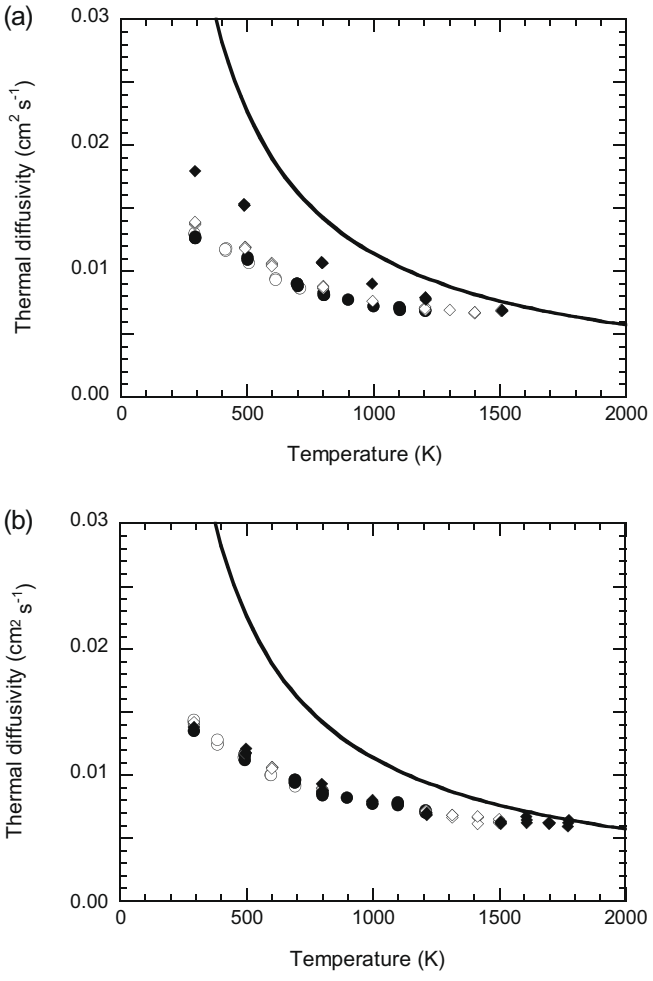


**Fig. 6.** Thermal diffusivities of samples 2 and 4. (a) Sample 2 and (b) sample 4. ○: Run 1, ●: Run 2, ◇: Run 3, ♦: Run 4. ——: unirradiated $UO_2$ [15].

Elastic strain density of dislocation per unit volume, $U_{disV}$, can be expressed as:

$$U_{disV} = \rho \cdot U_{dis} \tag{11}$$

where $\rho$ is the dislocation density per unit volume.

For irradiated $UO_2$, the strain energy densities induced by the accumulation of dislocations were calculated using the data shown in Table 3.

Regarding sample 2, the non-uniform strain increases while the lattice parameter decreases, compared to sample 1. As a consequence, the total strain energy density hardly changes in either sample, as seen in Fig. 10. It is likely that the decrease of uniform strain causes the increase of non-uniform strain in sample 2. On the other hand, the strain energy density of sample 4 decreases compared to that of sample 3: this is mainly due to the decrease of non-uniform strain which occurred in sample 4. It is considered that the annealing temperature during thermal diffusivity measurement affected the recovery behavior of strain energy density in the sample.

It is found that the strain energy densities of the two samples tend to be lower than the reported values which were measured on the samples irradiated in commercial reactors [2]. In consideration of the thermal conductivity recovery behaviors of the two samples, it is suggested that the decrease of strain energy density may be mainly caused by the recoveries of point defect and non-uniform strain which occurred during irradiation.

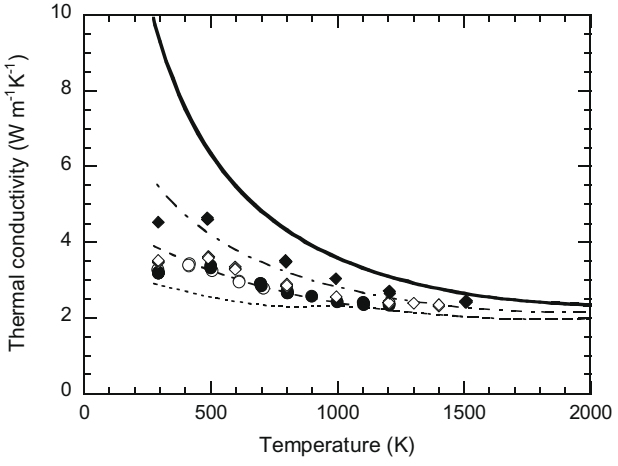


**Fig. 7a.** Thermal conductivities of sample 2 ○: Run 1, ●: Run 2, ◇: Run 3, ♦: Run 4. ——: unirradiated $UO_2$ [15]. - - -, – –, – · –: values calculated by using the formula in [10,16]; - - -: before point defect recovery, – – –: after point defect recovery, – · – : soluble FPs-doped $UO_2$ (simulated burnup: 60 GWd/t) [16].

### *4.3. Relationship between changes in the crystal lattice strain and thermal conductivity of irradiated $UO_2$ pellets*

As seen in Fig. 8, the lattice parameter of sample 1 is close to that of unirradiated $UO_2$. After annealing at about 1600 K, the

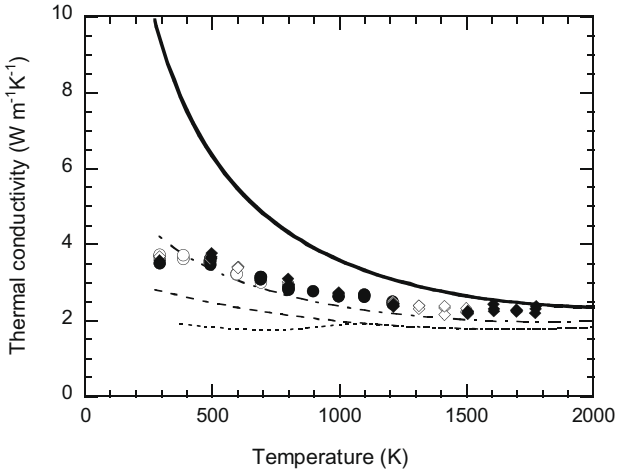


**Fig. 7b.** Thermal conductivities of sample 4. ○: Run 1, ●: Run 2, ◇: Run 3, ♦: Run 4. ——: unirradiated $UO_2$ [15]. - - -, – –, – · –: values calculated by using the formula in [10,16]; - - - ·: before point defect recovery, – – -: after point defect recovery, – · – ·: soluble FPs-doped $UO_2$ (simulated burnup: 130 GWd/t) [16].

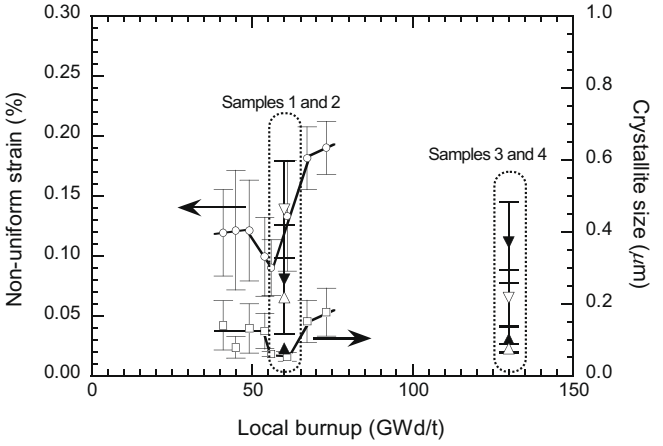


**Fig. 9.** Local burnup dependence of non-uniform strain and crystallite size in irradiated $UO_2$ samples. ▼, ▽: non-uniform strain (this study); ○: non-uniform strain (Amaya et al. [2]); ▼: as-irradiated; ▽: after thermal diffusivity measurement; ▲, △: crystallite size (this study); □: crystallite size (Amaya et al. [2]) ▲: as-irradiated; △: after thermal diffusivity measurement.

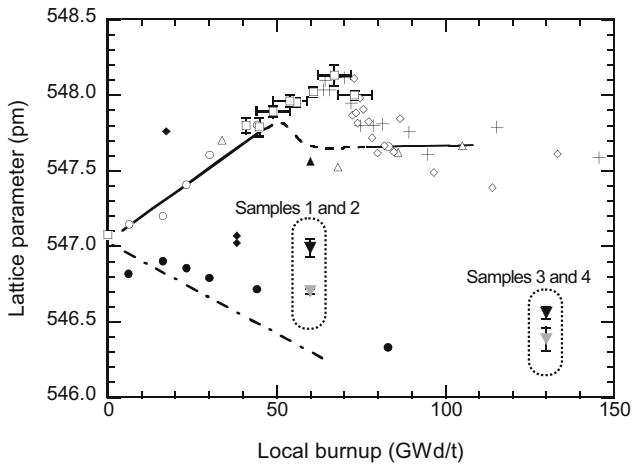


**Fig. 8.** Local burnup dependence of the lattice parameter of irradiated $UO_2$ samples. ▼, ▼: this study; ▼: as-irradiated; ▼: after thermal diffusivity measurement; ○, ——: Une et al. (irradiated) [17]; ●: Une et al. (annealed) [17]; △: Davies and Ewart [18]; ◇, +: Spino et al. [19]; ▲: Nogita et al. [20]; – · –: Une and Oguma [21]; □: Amaya et al. [2,22]; ♦: Minato et al. [23].

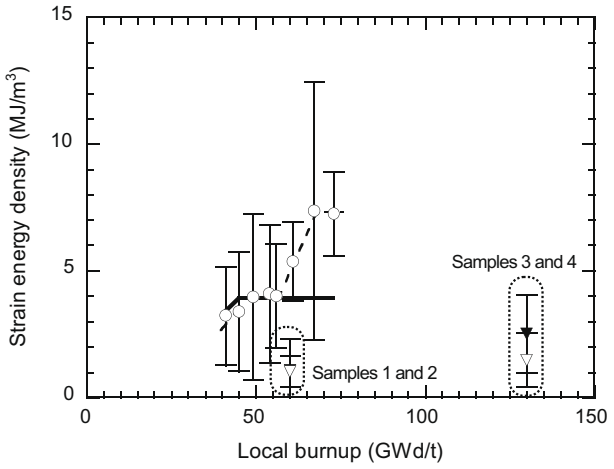


**Fig. 10.** Local burnup dependence of strain energy density of irradiated $UO_2$ samples. ▼, ▽: this study; ▼: as-irradiated; ▽: after thermal diffusivity measurement; ○: Amaya et al. [2]; – – –: the trend of the measured values [2]; ——: the value calculated from the dislocation densities [2].

**Table 3**
Data used in calculation of strain energy density due to accumulation of dislocation.

| | |
|---|---|
| Shear modulus $\mu$ [27] | 77 GPa |
| Burgers vector $b$ [25] | 0.39 nm |
| Poisson ratio $\nu$ [27] | 0.31 |
| Dislocation density $\rho$ [25] | $\log \rho = 2.2 \times 10^{-2}$ Bu + 13.8 (6 < Bu < 44 GWd/t) = 14.77 (Bu > 44 GWd/t) $\rho$ in m/m$^3$ and Bu in GWd/t) |
| Radius of stress region affected by dislocation $r_1$ | $1/\sqrt{\rho}$ |
| Radius of dislocation core $r_0$ | 0.55 nm (derived from the lattice parameter of $UO_2$ [20,21]) |

lattice parameter decreases as seen in the results of sample 2. Though the lattice parameter of sample 4 also shows a decrease after annealing at 1800 K compared to that of sample 3, the amount of lattice parameter decrease is less than that between samples 1 and 2. This trend of lattice parameter decrease is similar to that of thermal conductivity recovery.

In connection with the recovery behavior of thermal conductivity, the lattice parameter changes before and after the high temperature annealing of the samples can be explained as follows:

(1) Considering the changes in the lattice parameters and non-uniform strains, it is likely that the increase of non-uniform strain is caused by the decrease of uniform strain which is mainly due to a point defect recovery.
(2) As seen in Fig. 7a, thermal conductivity of irradiated $UO_2$ pellet recovers after being annealed at 1500 K during thermal diffusivity measurements. Crystallite size and non-uniform strain also increased after the thermal diffusivity measurements. It is considered that these phenomena occur in the temperature range from 1300 to 1600 K, and are mainly due to the migration of dislocations: dislocation tangle proceeds by the migration of dislocation, and high-angle grain boundaries generate gradually. Micro-bubbles with fission gas in the crystal grain also migrate with the migration of the high-angle grain boundary, and the fission gas bubble coarsens. As a result, thermal conductivity recovery occurs after being annealed at 1500 K.

## 5. Conclusion

Two kinds of disk-shaped $UO_2$ samples (4 mm in diameter and 1 mm in thickness) were irradiated in a test reactor up to about 60 and 130 GWd/t, respectively.

Microstructures of the samples were investigated by means of optical microscopy, scanning electron microscopy/ electron probe micro-analysis (SEM/EPMA) and micro-X-ray diffractometry. Based on the micro-X-ray diffraction results, lattice parameters and diffraction peak broadenings (increase of FWHM of diffraction peak) of the samples were obtained. Crystallite size and non-uniform strain between crystallites were evaluated from the increases of FWHM of the diffraction peaks using the Williamson–Hall method.

The measured lattice parameters tended to be considerably smaller than the reported values, and the typical cauliflower structure which is often observed in high burnup fuel pellets is hardly seen in these samples. In addition, many large pores were observed in sample 3. This suggests that the irradiation temperature of sample 3 was higher than the target temperature of 1273 K. On the other hand, the increase of pore size was not so significant in sample 1. It seems that the burnup of sample 1 did not reach the formation threshold of the high burnup structure. Measured crystallite sizes of irradiated samples were in the range of 50–200 nm and these were nearly the same as those of the sub-divided and/or recrystallized grains in the rim structure. Elastic strain energy densities in the samples were also evaluated based on the crystal lattice and non-uniform strain.

Thermal diffusivities of the samples were measured by using a laser flash method, and their thermal conductivities were evaluated by multiplying the heat capacity of unirradiated $UO_2$ and sample densities. While the thermal conductivities of sample 2 showed recovery after being annealed at 1500 K, those of sample 4 were not clearly observed even after being annealed at 1500 K. These trends suggest that the amount of accumulated irradiation-induced defects depends on the irradiation condition of each sample.

From the comparison of the changes in the lattice parameter and strain energy density before and after the thermal diffusivity measurements, it is likely that the thermal conductivity recovery in the temperature region from 1200 to 1500 K is related to the migration of dislocations: the migration of dislocations affects the changes in crystal lattice strain and crystallite size and causes the coarseness of micro-bubbles which contain fission gas.

## Acknowledgments

This work was carried out as a joint study by the JAEA (Japan Atomic Energy Agency)–MHI (Mitsubishi Heavy Industries, Ltd.). The authors were deeply indebted to Dr. K. Hayashi of JAEA for planning of this irradiation test. They thank their colleagues in the Fuel Safety Research Group, the members in the Department of Research Reactor and Tandem Accelerator for the irradiation test, and the members in the Reactor Fuel Examination Facility for their cooperation in the post irradiation examinations.

## References

[1] M. Kinoshita, T. Sonoda, S. Kitajima, et al., Proc. 2004 Int. Mtg LWR Fuel Perform., Paper 1102, September 19–22, Orlando, Florida, 2004.
[2] M. Amaya, J. Nakamura, T. Fuketa, J. Nucl. Sci. Technol. 44 (2008) 255.
[3] M. Amaya, J. Nakamura, T. Fuketa, J. Nucl. Mater. 392 (2009) 439.
[4] K. Okumura, K. Kaneko, K. Tsuchihashi, SRAC95; General Purpose Neutronics Code System, JAERI-Data/Code 96-015, Japan Atomic Energy Research Institute, 1996.
[5] I. Owada, Y. Nishino, T. Kushida, J. Nakamura, T. Matsuda, Characterization test of the pellet thermal conductivity measurement apparatus using unirradiated samples, Japan Atomic Energy Research Institute, Report JAERI-Tech 94-028, 1994.
[6] Y. Takahashi, I. Yamamoto, T. Ohsato, Netsu-Sokutei 15 (1988) 103 (in Japanese).
[7] A. Cezairliyan, T. Baba, R. Taylor, Int. J. Thermophys. 15 (1994) 317.
[8] SCDAP/RELAP5-3D Code Development Team, INEEL/EXT-02-00589, May 2002.
[9] K. Nogita, K. Une, J. Nucl. Sci. Technol. 30 (1993) 900.
[10] M. Amaya, M. Hirai, H. Sakurai, K. Ito, M. Sasaki, T. Nomata, K. Kamimura, R. Iwasaki, J. Nucl. Mater. 300 (2002) 57.
[11] T. Takahashi, Imono 65 (1993) 13 (in Japanese).
[12] G.K. Williamson, W.H. Hall, Acta Metal. 1 (1953) 22.
[13] A.G. Croff, Nucl. Technol. 62 (1983) 335.
[14] R. Brandt, G. Neuer, J. Non-Equilib. Thermodyn. 1 (1976) 3.
[15] S. Ishimoto, M. Hirai, K. Ito, Y. Korei, J. Nucl. Sci. Technol. 31 (1994) 796.
[16] M. Amaya, M. Hirai, J. Nucl. Mater. 247 (1997) 76.
[17] K. Une, K. Nogita, S. Kashibe, et al., J. Nucl. Mater. 188 (1992) 65.
[18] J.H. Davies, F.T. Ewart, J. Nucl. Mater. 41 (1971) 143.
[19] J. Spino, D. Papaioannou, J. Nucl. Mater. 281 (2000) 146.
[20] K. Nogita, K. Une, M. Hirai, et al., J. Nucl. Mater. 248 (1997) 196.
[21] K. Une, M. Oguma, J. Nucl. Sci. Technol. 20 (1983) 844.
[22] M. Amaya, K. Une, M. Hirai, J. Nucl. Sci. Technol. 41 (2004) 108.
[23] K. Minato, T. Shiratori, H. Serizawa, et al., J. Nucl. Mater. 288 (2001) 57.
[24] K. Nogita, K. Une, J. Nucl. Mater. 226 (1995) 302.
[25] K. Nogita, K. Une, Nucl. Inst. Meth. Phys. Res. B. 91 (1994) 301.
[26] T. Yokobori, et al., Kinzokuzairyou-No-Kyoudo-To-Hakai, Nippon-Kinzoku-Gakkai-Kyoudo-Iinkai, Maruzen, Tokyo, 100 (1964) (in Japanese).
[27] A. Padel, Ch. de Novion, J. Nucl. Mater. 33 (1969) 40.